# Hydrogen-induced defects in bulk niobium

Jakub Čížek,* Ivan Procházka, František Bečvář, Radomír Kužel, and Miroslav Cieslar
*Faculty of Mathematics and Physics, Charles University, V Holešovičkách 2, CZ-18000, Praha 8, Czech Republic*

Gerhard Brauer and Wolfgang Anwand
*Institut für Ionenstrahlphysik und Materialforschung, Forschungszentrum Rossendorf, Postfach 510119, D-01314 Dresden, Germany*

Reiner Kirchheim and Astrid Pundt
*Institut für Materialphysik, Universtät Göttingen, Tammannstrasse 1, D-37073 Göttingen, Germany*
(Received 23 June 2003; revised manuscript received 9 January 2004; published 23 June 2004)

Our aim in the present work was to investigate changes of the defect structure of bulk niobium induced by hydrogen loading. The evolution of the microstructure with increasing hydrogen concentration was studied by x-ray diffraction and two complementary techniques of positron annihilation spectroscopy (PAS), namely positron lifetime spectroscopy and slow positron implantation spectroscopy with the measurement of Doppler broadening, in defect-free Nb (99.9%) and Nb containing a remarkable number of dislocations. These samples were electrochemically loaded with hydrogen up to $x_H = 0.06$ [H/Nb], i.e., in the $\alpha$-phase region, and it was found that the defect density increases with hydrogen concentration in both Nb samples. This means that hydrogen-induced defects are created in the Nb samples. A comparison of PAS results with theoretical calculations revealed that vacancy-hydrogen complexes are introduced into the samples due to hydrogen loading. Most probably these are vacancies surrounded by 4 hydrogen atoms.

DOI: 10.1103/PhysRevB.69.224106 PACS number(s): 78.70.Bj, 61.72.−y

## I. INTRODUCTION

The hydrogen behavior in metals has been studied for many years. On the one hand, it is interesting from the theoretical point of view, because it is a very close physical realization of the theoretical lattice-gas model. On the other hand, hydrogen storage in metals is of considerable technological importance for practical applications.

A very interesting property of hydrogen atoms in metals is their high mobility at room temperature.[1] The high mobility increases the probability of interaction between hydrogen atoms and defects. It is known that hydrogen in metals leads to a worsening of mechanical properties, e.g., embrittlement, crack formation, etc.[2] For this reason, it is very important to learn about the mechanism of interaction between hydrogen and defects of a crystalline structure, which is still not completely understood. In particular data about hydrogen interaction with defects on the atomic scale are still rather incomplete despite the increasing effort given to such investigations.

It is known that there is a positive binding energy between hydrogen and a vacancy. Hydrogen trapping in vacancies in Cu was experimentally observed by Lengeler *et al.*[3] by means of positron annihilation spectroscopy (PAS). They find that hydrogen is bound to a vacancy in Cu by at least 0.4 eV. This experimental binding energy is in good agreement with effective medium theory calculations.[4] As another example, it was found that hydrogen atoms in plastically deformed Pd segregate at dislocations.[5] Thus the behavior of hydrogen in metals is strongly affected by the presence of defects.

Hydrogen is not only trapped at existing defects, but new defects could be also created due to hydrogen loading. An increase of the S parameter was observed in hydrogen loaded Pd compared to a virgin sample in measurements of angular correlation curves of positron annihilation quanta.[6] It can be interpreted as an increase of the defect density due to hydrogen loading. Recently a huge increase of the defect density in hydrogenated $LaNi_5$ hydrogen storage alloy was observed by Shirai *et al.* in Ref. 7. The authors have found dislocations and a large number of excess vacancies introduced into the alloy due to hydrogen loading.

Hence, there seems to be some indications of hydrogen-induced defects in metals even in $\alpha$-phase H-metal systems. However, this effect still needs to be clarified. One should note that in both experimental findings mentioned above the hydrogen concentrations in the samples were unknown. Moreover, in the case of $LaNi_5$ alloy the situation is more complicated due to hydride formation, which can be itself connected with the creation of new defects.[8,9] In addition, the behavior of hydrogen-induced defects as a function of the hydrogen concentration in the sample has not been studied so far. Also the nature of the hydrogen-induced defects is still not completely clarified. For example it is a question whether in all cases vacancies together with dislocations are created. Another open question is whether the created vacancies are free or associated with hydrogen atoms as vacancy–hydrogen pairs or even vacancy–hydrogen complexes.

Therefore, in the present work we decided to study defects in hydrogenated Nb in order to obtain more data about this interesting phenomenon, which could help in its physical interpretation. We choose Nb because it is a widely studied material in connection with hydrogen, and the hydrogen behavior in Nb is well known. Hydrogen first fills the tetrahedral interstitial sites in the bcc lattice of Nb. At room temperature the Nb–H system represents a single phase solid solution (the so called $\alpha$-phase) up to a hydrogen concentration $x_H = 0.06$ [atomic ratio H/Nb]; see Ref. 8. At higher hy-

 

drogen concentrations the system becomes a mixture of two phases: the $\alpha$-phase and the hydrogen-rich $\beta$-phase, which is an orthorombic distortion of the bcc Nb lattice.

In the present work we studied defects in hydrogenated Nb as a function of hydrogen concentration. The investigations were performed up to $x_H = 0.06$ [H/Nb], i.e., only in the single phase region. Thus, we avoided the defects, which could be introduced into Nb due to precipitation of the $\beta$-phase. Our aim in the present work was to give answers to the following questions: (1) Which defects are created due to hydrogen loading? (2) How does the population of hydrogen-induced defects depend on the hydrogen concentration in the sample? (3) How do defects already present in the virgin sample influence the process of hydrogen-induced defects creation? To be successful in these tasks we studied three sets of Nb samples. Each set exhibited a different amount of defects already present in the virgin samples. A comparison of these samples can give us information how the initial defect structure influences the hydrogen behavior. All samples were step-by-step electrochemically loaded by hydrogen to monitor the behavior of defects with increasing hydrogen concentration. Defect studies were performed by two complementary techniques of positron annihilation spectroscopy (PAS), namely positron lifetime (PL) spectroscopy and slow positron implantation spectroscopy (SPIS) with measurement of Doppler broadening. PAS represents a well established nondestructive and nonlocal technique with a high sensitivity to open volume defects like vacancies, vacancy clusters, dislocations, etc.[10] SPIS enables us to study the depth profile of defects using a monoenergetic positron beam with adjustable positron energy.[11] Thus, PAS represents a valuable tool for defect studies in metals containing hydrogen. Experimental results were directly correlated with theoretical calculations of positron lifetimes for various defect configurations. PAS investigations were combined with x-ray diffraction (XRD) measurements.

The paper is structured as follows: Experimental details are given in Sec. II. The characterization of virgin Nb samples can be found in Sec. III A, while in Sec. III B we describe the experimental results obtained on hydrogenated samples. The results of theoretical calculations are presented in Sec. IV and final conclusions are drawn in Sec. V.

## II. EXPERIMENTAL

### A. Nb samples

Disk shaped specimens of 10 mm diameter and a thickness of 1 mm were cut from the rod of pure Nb (99.9%) purchased from Mateck GmbH. Tantallum with a concentration around 300 wt. ppm is the main impurity in the Nb samples. Ta atoms are fully dissolved in Nb. The concentration of all other impurities lie below 10 wt. ppm. Specimens with different microstructures were prepared: (a) *As-received sample*. This sample represents material plastically deformed during preparation and shaping in the company and parameters of the plastic deformation are not known. An additional deformation was introduced by cutting of the disks and surface polishing. (b) *Sample annealed at 850 °C*. In order to recover the defects present in the as-received sample, one set of samples was annealed at 850 °C for 1 hour. The annealing was performed in a high vacuum of $10^{-6}$ mbar and the annealed samples were slowly cooled within the furnace. This annealing leads to partial recovery of defects as will be shown in Sec. III A. (c) *Sample annealed at 1000 °C*. Another set of samples was annealed at 1000 °C for 1 hour. The samples were encapsulated into an evacuated ($p = 10^{-2}$ mbar) capsule made from quartz glass. The annealed samples were slowly cooled within the furnace. This resulted in a complete recovery of defects as will be discussed in Sec. III A. (d) *Sample quenched from 1000 °C*. A last set of samples was annealed at 1000 °C for 1 hour in the same way as the previous one. However, the annealing was finished by a rapid quenching into water of room temperature. The samples contain quenched-in excess vacancies as will be explained in Sec. III A.

The as-received Nb sample (a), the Nb sample (b), i.e., annealed at 850 °C, and the Nb sample (c), i.e., annealed at 1000 °C, were chosen for the hydrogen loading experiment. Both sides of each sample were covered by a thin Pd overlayer with a thickness of 30 nm to protect Nb from oxidation and to facilitate the hydrogen doping. The thin Pd overlayer was sputtered by dc magnetron sputtering. The sputtering was performed at room temperature with a sputtering rate of 1.9 nm/min and the pressure of Ar around $10^{-4}$ mbar. The residual pressure in the sputtering chamber was $10^{-10}$ mbar. Prior sputtering of the thin Pd overlayer, the samples were exposed to an Ar beam for 10 min to clean the surface and to remove an oxide layer (if any). In case of the annealed samples the thin Pd overlayer was sputtered after the annealing.

### B. Hydrogen loading

Hydrogen loading was performed using step-by step electrochemical charging with constant current pulses.[5] The current density was $3.8 \times 10^{-3}$ mA mm$^{-2}$. This current density results in hydrogen charging rate (number of introduced hydrogen atoms per unit of area and time) $2 \times 10^{13}$ H atoms mm$^{-2}$ s$^{-1}$. The hydrogen diffusion coefficient in Nb at room temperature $D = 4 \times 10^{-6}$ cm$^2$ s$^{-1}$ can be derived from literature.[12] Hence, the increase of the volume concentration of H atoms in the near-surface region during the electrochemical charging is $1.2 \times 10^{15}$ mm$^{-3}$ per second. It corresponds to the increase of the H to Nb atom ratio of $2 \times 10^{-8}$ H/Nb per second. The combination of such moderate charging rate and high hydrogen mobility at room temperature results in virtually no excess of hydrogen concentration in the near-surface region during charging. It was proved by depth profile measurements by means of SPIS, see Sec. III B as well as by the same results of XRD on both sides of the samples. We used a mixture of $H_3PO_4$ (85%) and glycerin (85%) in the ratio 1:1 as an electrolyte. In order to prevent hydrogen losses, oxygen was removed from the electrolyte by slow bubbling with Ar for 24 hours prior to electrochemical charging. The hydrogen concentration in the sample was calculated from the electric charge by Faraday's law.[13]

### C. Experimental methods

X-ray diffraction measurements were taken in $\Theta/2\Theta$ geometry with HZG4 (Seifert-FPM) and Philips X'pert MPD

TABLE I. Lattice parameter $a$ obtained from XRD spectra for the studied Nb samples.

| Sample | $a$ (Å) |
|---|---|
| Nb as received | 3.3071(4) |
| Nb annealed 850°C/1 h | 3.3025(3) |
| Nb annealed 1000°C/1 h | 3.3029(3) |

diffractometers using Cu-$K_\alpha$ and Co-$K_\alpha$ radiation. The XRD profiles were fitted with the Pearson VII function and the lattice parameters were determined by the Cohen–Wagner extrapolation plot ($a_{hkl}$ vs cos $\Theta$ cot $\Theta$).

A fast–fast PL spectrometer similar to that described in Refs. 14 and 15 was employed in the present work. A positron source of ~1.3 MBq activity sealed between two mylar foils of 2 $\mu$m thickness was used. The timing resolution of the spectrometer was 150 ps (FWHM) for $^{22}$Na at a typical coincidence count rate of 80 $s^{-1}$. At least $10^7$ counts were collected in each PL spectrum. Measured spectra were decomposed by means of a maximum-likelihood procedure.[16] The time-resolution function of the spectrometer was considered to be a sum of three Gaussians and was fitted simultaneously with the other parameters (for details see Refs. 14 and 16).

SPIS was performed on the magnetically guided system "SPONSOR" at Forschungszentrum Rossendorf.[17] Positron energies between 0.030 and 35 keV were used. Energy spectra of annihilation gamma rays were measured with a Ge detector having an energy resolution (FWHM) of 1.09±0.01 keV at 511 keV. The diameter of the spot of the beam was ≈4 mm. The S-E dependencies were fitted by the program VEPFIT.[18]

TEM observations of microstructure were performed on the JEOL 2000 FX electron microscope operating at 200 kV with EDX system LINK AN 10000. Thin foils for TEM were prepared by ion milling.

## III. RESULTS AND DISCUSSION

### A. Virgin samples

Peaks corresponding to Nb reflections were found in the XRD spectra of the studied samples. In addition, a very weak and broad (111) peak corresponding to the thin Pd overlayer was detected. The lattice constants obtained from the XRD spectra for the studied Nb samples are listed in Table I. The lattice parameter for Nb $a=3.3033(1)$ Å can be found in the PDF-2 database.[19] Clearly, the lattice parameters measured on the annealed samples exhibit reasonable agreement with the PDF-2 value. On the other hand, the lattice parameter for the as-received sample is remarkably higher than the literature value. We have found that it is due to macroscopic strains, which are present in the as-received sample. It can be well seen from the results of $\Psi$-stress measurements plotted in Fig. 1. The position of the (310) Nb peak was measured at various angles $\Psi$ between the scattering vector and the normal to the surface of the sample. The condition of the Bragg

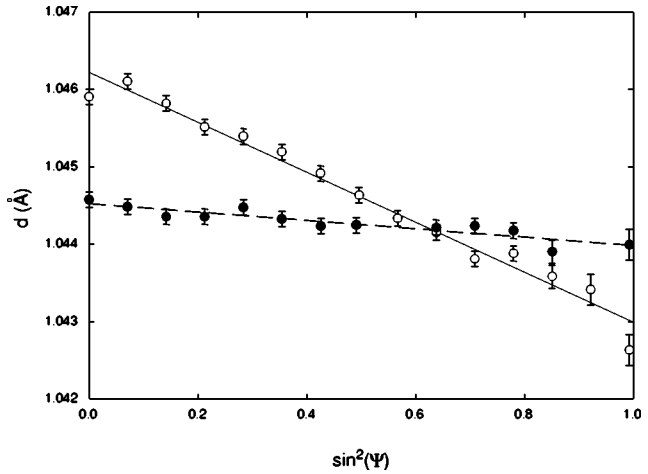


FIG. 1. The inter-plane distance $d$ of the (310) planes as a function of $\sin^2 \Psi$. The tilting angle $\Psi$ represents the angle between the scattering vector and normal to the surface of the sample. The dependence of $d$ on $\sin^2 \Psi$ is plotted by open circles for the as-received Nb sample and by full circles for the Nb sample annealed at 1000°C. A linear fit of the experimental points is shown by the solid lines.

diffraction of the (310) plane requires that the scattering vector is aligned with the normal to this plane. Thus, the Bragg reflections from the (310) planes with various angles between their normal and the normal to the surface of the sample can be measured by tilting the sample by various $\Psi$ angles. The distance between the (310) planes calculated from the position of the (310) peak is plotted in Fig. 1 as a function of the angle $\Psi$. It can be shown that under the condition that the stress component perpendicular to the surface of the sample $\sigma_3=0$, the distance between the (310) planes measured for sample tilted by angle $\Psi$ is linearly proportional to $\sin^2 \Psi$. As one can see in Fig. 1 it is the case for the as-received Nb sample. Hence, we can conclude that the as-received Nb sample contains macroscopic compressive strain. Assuming single-axis strain, we can estimate the compressive stress in the sample $\sigma=-250$ MPa. The strain was introduced into the sample most probably during cutting of the disk-shaped samples and/or by subsequent polishing of the sample surface. The dependence of the distance between the (310) planes on the tilting angle $\Psi$ for the Nb sample annealed at 1000°C for 1 h is also plotted in Fig. 1 for a comparison. Contrary to the as-received sample, the distance between the (310) planes for the sample annealed at 1000°C exhibits only a very slight change with the tilting angle $\Psi$. Hence, the macroscopic strain was relaxed during annealing.

The PL results for the studied Nb samples are listed in Table II. The Nb sample annealed at 1000°C for 1 hour exhibits a single-component PL spectrum with lifetime $\tau_1=128.3\pm0.4$ ps. It agrees well with the experimental as well as theoretically calculated bulk positron lifetime $\tau_B$ in Nb reported in the literature;[20] see also Sec. IV. It means that defects present in the as-received sample are completely recovered during annealing at 1000°C. The annealed sample exhibits a very low defect density, which falls below the resolution limit of PL spectroscopy,[21] i.e., a vacancy concen-

TABLE II. Lifetimes $\tau_i$ and relative intensities $I_i$ found in PL spectra of the studied Nb samples. The lifetimes $\tau_2=153$ ps and $\tau_3=222$ ps were kept fixed during the decomposition of PL spectrum of the as-received Nb sample; see the text. One standard deviations of the determined lifetimes and intensities are given in parentheses.

| Nb sample | $\tau_1$ (ps) | $I_1$ (%) | $\tau_2$ (ps) | $I_2$ (%) | $\tau_3$ (ps) | $I_3$ (%) |
|---|---|---|---|---|---|---|
| As-received | 61(7) | 14.6(6) | 153 fix | 61.7(9) | 222 fix | 23.7(9) |
| Annealed at 850°C for 1 h | 109(4) | 47(9) | 153(4) | 53(9) | – | – |
| Annealed at 1000°C for 1 h | 128.3(4) | 100 | – | – | – | – |
| Annealed at 1000°C for 1 h and quenched | 120(1) | 85(3) | 210(10) | 15(3) | – | – |

tration $c_v<10^{-6}$ at.% and a dislocation density $\varrho<10^{12}$ m$^{-2}$. Hence, we can consider this sample as a defect-free material.

The PL spectrum of the Nb sample quenched from 1000°C is well fitted by two exponential components; see Table II. The lifetime $\tau_1$ lies below the Nb bulk lifetime. Therefore, the first component with the lifetime $\tau_1$ comes from annihilations of free positrons. On the other hand, the second component represents the contribution of positrons trapped at defects. The lifetime $\tau_2$ exhibits good agreement with the lifetime of positrons trapped at Nb vacancies (222 ps) calculated in Sec. IV. Hence, the component with the lifetime $\tau_2$ comes from positrons trapped at quenched-in excess vacancies in the sample. These excess vacancies represent a fraction of thermal equilibrium vacancies present in the sample at 1000°C, which have been "frozen" in the sample due to rapid quenching down to room temperature.

The PL spectrum of the sample annealed at 850°C for 1 hour consists of two exponential components as well; see Table II. In similar way as for the previous sample, the first component with lifetime $\tau_1$ can be attributed to free positrons, while the second one with lifetime $\tau_2$ comes from positrons trapped at defects. Clearly, the lifetime $\tau_2$ is remarkably lower than the lifetime of positrons trapped in Nb vacancies. It is typical for positrons trapped at dislocations. It should be noted that it is generally accepted that a dislocation line itself represents only a shallow positron trap. Once a positron is trapped at a dislocation line, it diffuses rapidly along the dislocation and is eventually trapped at some deep trap, usually a vacancy anchored in the elastic field of the dislocation.[22] Clearly a vacancy bound to a dislocation line exhibits a slightly smaller free volume due to the elastic stress field of the dislocation. As a consequence, the lifetime of positrons trapped at dislocations by the process described above is shorter than the lifetime of positrons trapped in a free monovacancy. Thus, we can assume that the component with the lifetime $\tau_1$ represents the contribution of positrons trapped at dislocations. This interpretation is supported by the fact that these defects have a relatively high thermal stability as they are not annealed out after heating of the sample at 850°C.

The two-component decomposition of the PL spectrum of the as-received Nb sample resulted in a free positron component with lifetime $\tau_1=94\pm4$ ps and a component with lifetime $\tau_2=186\pm2$ ps which can be attributed to positrons trapped at defects. The lifetime $\tau_2$ is, on one hand, higher than the lifetime of positrons trapped at Nb dislocations, on the other hand, it is lower than the lifetime of positrons trapped at Nb vacancies. One can expect that dislocations as well as vacancies were created in the as-received sample due to plastic deformation. The fact that excess vacancies were found in the sample quenched from 1000°C indicates that the excess vacancies are quite stable in Nb at room temperature. Both, positrons trapped at dislocations and positrons trapped at vacancies, contribute to the component with the lifetime $\tau_2$. Thus, the lifetime $\tau_2$ represents an effective lifetime due to the simultaneous presence of these two kinds of defects.

To separate the contributions of these two kinds of defects, we performed a decomposition of the PL spectrum of the as-received Nb sample into three components. Lifetimes $\tau_2=153$ ps of positrons trapped at dislocations and $\tau_3=222$ ps of positrons trapped at vacancies were kept fixed. Results of this decomposition are shown in Table II. The decomposition gives a good fit of the PL spectrum of the as-received Nb sample.

Thus, we can conclude that the as-received Nb sample contains dislocations and vacancies, which were created due to plastic deformation during machining, cutting and surface polishing. TEM investigations of the as-received Nb sample revealed the grain size in range (10−15) $\mu$m. No defects except of radiation damage due to ion milling employed in the foil preparation were observed by TEM. It should be pointed out that the TEM foils represents a microstructure in depth at half of the sample thickness. Hence, the obtained results corresponds well with the picture that the defects detected by PAS in the as-received sample were created by cutting and polishing and are situated in a layer relatively close to the sample surface. Annealing of the sample at 850°C results in the recovery of vacancies which anneal out, i.e., the Nb sample contains only dislocations. Further heating of the sample at higher temperatures leads to the recovery of dislocations. As a consequence, a complete recovery of defects occurred in the sample annealed at 1000°C and it can be considered as defect-free.

### B. Hydrogen loaded samples

The studied samples were step-by-step charged with hydrogen. The increase of the hydrogen concentration leads to an increase of the sample volume and, therefore, also an increase of the lattice constant. The relative lattice expansion

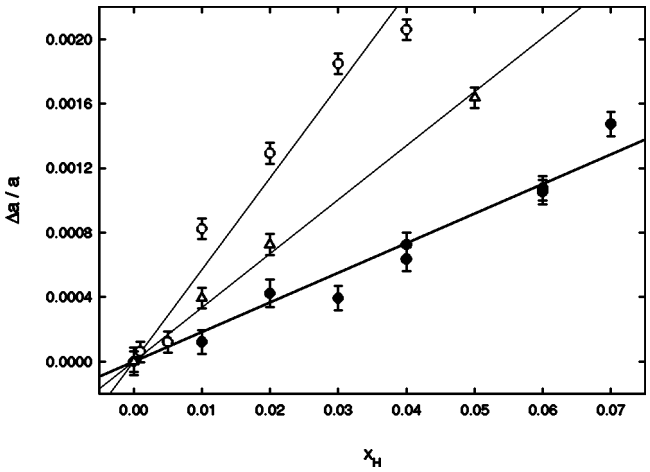


FIG. 2. The relative lattice expansion $\Delta a/a_0$, $\Delta a = a - a_0$, as a function of the hydrogen concentration $x_H$. $a_0$ and $a$ denote the lattice constant for a virgin sample and a sample with a hydrogen concentration $x_H$, respectively. The relative lattice expansion for the as-received sample is plotted by full circles. Open triangles are used to show the relative lattice expansion for the Nb sample annealed at 850°C, and the relative lattice expansion for the Nb sample annealed at 1000°C is plotted by open circles. A linear fit of the experimental data is shown by the solid lines.

in the $\alpha$-phase is directly proportional to the hydrogen concentration in the sample

$$\frac{a - a_0}{a_0} = \xi x_H. \tag{1}$$

The symbol $a$ states for the lattice constant of a sample with hydrogen concentration $x_H$ [H/metal atom ratio], while $a_0$ denotes the lattice constant of a hydrogen-free virgin sample. The coefficient $\xi = 0.058$ can be found in the literature for bulk Nb.[23]

The relative lattice expansions for the studied Nb samples obtained from XRD data are plotted in Fig. 2 as a function of hydrogen concentration. One can see in Fig. 2 that the lattice indeed expands linearly with hydrogen concentration in all the studied samples. However, the slope of the linear increase differs from sample to sample. For the Nb sample annealed at 1000°C, i.e., the defect-free specimen, the parameter $\xi = 0.058 \pm 0.004$ was obtained from a linear fit of the experimental data. Clearly, this value agrees well with the literature.[23]

On the other hand, the Nb sample annealed at 850°C exhibits the parameter $\xi = 0.037 \pm 0.004$, which is remarkably lower than that for the defect-free sample. The smallest parameter $\xi = 0.017 \pm 0.004$ was found for the as-received Nb sample. Thus, a higher defect density in a sample results in a lower coefficient $\xi$ for the lattice expansion. The lower lattice expansion for the samples with defects can be explained by the segregation of hydrogen atoms at dislocations.[5,24] Volume expansion due to a hydrogen atom segregated at a dislocation is significantly lower than that of a hydrogen atom situated at an interstitial position in the defect-free lattice. A similar situation occurs also for a hydrogen trapped at a vacancy.

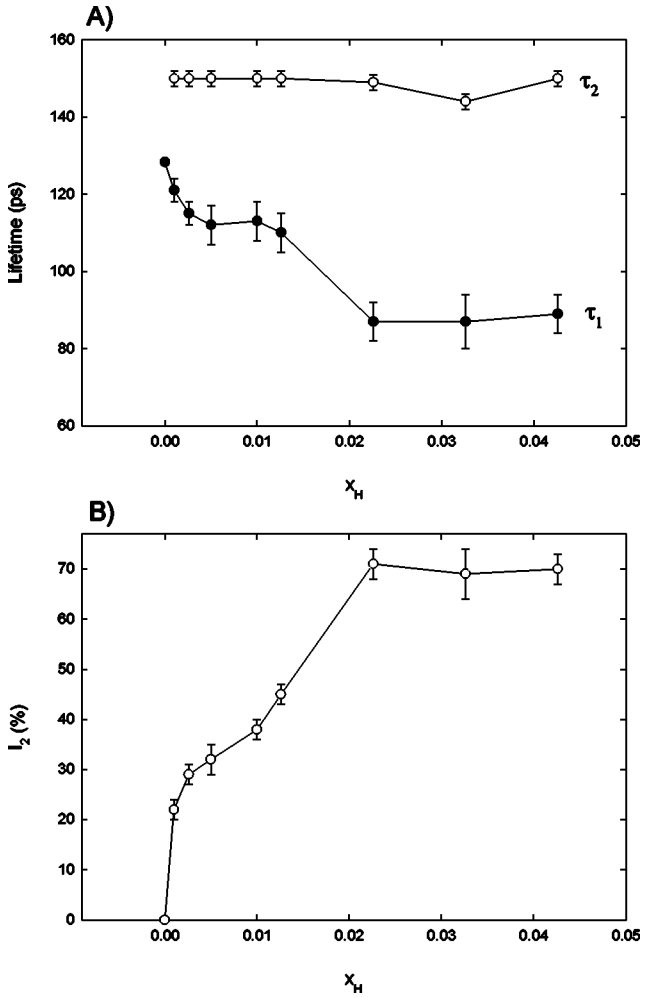


FIG. 3. (a) The lifetimes $\tau_1$ and $\tau_2$ of the exponential components resolved in PL spectra for the Nb sample annealed at 1000°C as a function of hydrogen concentration $x_H$. (b) Dependence of the relative intensity $I_2$ on hydrogen concentration for the Nb sample annealed at 1000°C.

No indication of the appearance of the $\beta$-phase was found in the XRD spectra of the studied samples loaded below a hydrogen concentration $x_H = 0.07$. Thus, in the hydrogen concentration range, where the defect study is performed, the samples represent a single-phase solid solution. The peaks of the orthorombic NbH phase were first observed in the XRD spectra of the samples loaded at a hydrogen concentration $x_H = 0.07$.

Lifetimes of exponential components resolved in PL spectra of the Nb sample annealed at 1000°C are plotted in Fig. 3(a) as a function of the hydrogen concentration $x_H$[H/Nb]. One can see in Fig. 3(a) that a new component with lifetime $\tau_2 \approx 150$ ps appeared in the PL spectrum already for the sample loaded to a hydrogen concentration $x_H = 0.001$. It is direct evidence that some new defects were created in the sample due to hydrogen loading. The lifetime $\tau_2$ does not change with hydrogen concentration. It means that the type of these hydrogen-induced defects remains the same during hydrogen loading. The dependence of the relative intensity $I_2$ of the new defect component on hydrogen concentration is

plotted in Fig. 3(b). One can see that the relative intensity $I_2$ increases significantly with increasing hydrogen concentration. It clearly indicates that the concentration of hydrogen-induced defects increases with increasing hydrogen concentration in the sample.

The lifetime of the hydrogen-induced defects $\tau_2 \approx 150$ ps lies substantially below the lifetime of positrons trapped in a monovacancy ($\tau_v = 222$ ps; see Sec. IV). The free volume of the hydrogen-induced defects is, therefore, remarkable smaller than the free volume of a Nb monovacancy. A natural explanation of the relatively small lifetime $\tau_2$ is that the defects created by hydrogen loading are associated with hydrogen. Most probably vacancies are created due to hydrogen loading. There is a positive binding energy between a vacancy and a hydrogen atom. As a consequence, the hydrogen-induced vacancies are coupled with one or more hydrogen atoms. The free volume of such vacancy–hydrogen complexes is reduced which is reflected by a lower lifetime $\tau_2$ of trapped positrons. This interpretation is supported from a drop of the monovacancy lifetime due to the decoration of monovacancies with hydrogen observed in tungsten.[25] Positron trapping in the vacancy–hydrogen complexes will be discussed in detail in Sec. IV. The volume expansion due to hydrogen absorption in the $\alpha$-phase concentration region is a reversible process and no plastic deformation of the sample takes place. Therefore, we do not assume that any dislocations were created by the hydrogen loading. However, even if some dislocations were introduced into the sample, anyway the lifetime of positrons trapped at the dislocations reflects the free volume of a vacancy bound to a dislocation line as was explained in Sec. III A. It means that in any case hydrogen-induced vacancies must be present in the hydrogenated sample. Hence, we can conclude that vacancy–hydrogen complexes are created in the sample annealed at 1000 °C due to hydrogen loading and the concentration of these hydrogen-induced defects increases with the hydrogen concentration.

The concentration of the hydrogen-induced vacancy-hydrogen complexes can roughly be estimated using the two state positron trapping model.[21] The model assumes a material with a single type of homogeneously distributed defects. Moreover, a transition limited trapping of thermalized positrons only is assumed and no detrapping of positrons is considered; see Refs. 21 and 26 for details. A quantity $\tau_f$ can be calculated from lifetimes and relative intensities of the exponential components resolved in the PL spectrum using the relation

$$\frac{1}{\tau_f} = \frac{I_1}{\tau_1} + \frac{I_2}{\tau_2}, \tag{2}$$

where $\tau_1$ represents lifetime of the free positron component and $\tau_2$ stands for lifetime of positrons trapped at a corresponding type of defects. Relative intensities of the free positron and the trapped positron component are denoted $I_1$ and $I_2$, respectively. If the assumptions of the two state trapping model are satisfied, then $\tau_f$ equals to the bulk positron lifetime $\tau_B$, i.e., the lifetime of free positrons in defect-free material. In niobium we found $\tau_B = 128.3 \pm 0.4$ ps; see Sec. III A. The quantity $\tau_f$ for the sample annealed at 1000 °C agrees well with the positron bulk lifetime $\tau_B$ in Nb during the whole measured range of hydrogen concentrations. Thus, the assumptions of the two state simple trapping model are fulfilled. The concentration $c$ of the hydrogen-induced defects can then be calculated using the equation

$$c = \frac{1}{\nu_{\mathrm{H-v}}} \frac{I_2}{I_1} \frac{\tau_2 - \tau_B}{\tau_B \tau_2}, \tag{3}$$

where $\nu_{\mathrm{H-v}}$ denotes the specific trapping rate for the vacancy–hydrogen complex. This quantity is not known at present, but it should be slightly lower than the specific trapping rate for the Nb monovacancy. Unfortunately, the latter has not been reported in literature so far. Thus, as a very rough estimation we can approximate that $\nu_{\mathrm{H-v}}$ lies in the range from $10^{14}$ s$^{-1}$ at. to $10^{15}$ s$^{-1}$ at., which is typical for such defects in metals.[21] From Eq. (3) we obtain that the concentration of hydrogen-induced vacancy–hydrogen complexes in the sample with a hydrogen concentration $x_{\mathrm{H}} = 0.04$ lies in the range $(0.3-3) \times 10^{-3}$ at.%. Thus, the number of the hydrogen-induced defects is substantially lower than the hydrogen concentration in the sample. From this, it follows that the majority of hydrogen atoms in the sample is situated in the regular tetrahedral interstitial positions of the Nb lattice and is not associated with vacancies.

The behavior of the positron lifetimes $\tau_1$ and $\tau_2$ for the Nb sample annealed at 850 °C with increasing hydrogen concentration is shown in Fig. 4(a). The dependence of the relative intensity of trapped positrons, $I_2$, on the hydrogen concentration is plotted in Fig. 4(b). Similarly to the previous sample, the intensity $I_2$ significantly increases with the hydrogen concentration. It indicates that new defects are created in the sample due to hydrogen loading in the same way as in the previous sample. The concentration of the hydrogen-induced defects goes up with the hydrogen concentration. Note that two kinds of defects exist in the sample annealed at 850 °C loaded with hydrogen: (a) dislocations already present in the virgin sample and (b) hydrogen-induced vacancy–hydrogen complexes. The lifetimes of positrons trapped at these two kinds of defects are too close to each other to be distinguished in the PL spectrum. Thus, the estimated lifetime $\tau_2$ gives an effective lifetime representing both defect components. The increasing ratio of the hydrogen-induced defects to dislocations with an increasing hydrogen concentration could be reflected by a slight decrease of $\tau_2$; see Fig. 4(a).

One can see in Figs. 3 and 4 that loading of the samples above $x_{\mathrm{H}} \sim 0.03$ does not result in a further increase of $I_2$, i.e., some kind of saturation of the concentration of hydrogen-induced defects can be observed.

A hydrogen-loaded as-received Nb sample has not been measured by PAS due to its more complex population of defects in the virgin state.

The Nb samples were studied also by means of SPIS. Varying the energy of the positron beam allows us to study the depth profile of defects. The dependence of the $S$ parameter on the positron energy $E$ for the virgin Nb sample annealed at 1000 °C is plotted in Fig. 5. Note that this sample was measured prior to sputtering of the thin Pd overlayer. One can see in Fig. 5 that $S$ decreases with positron energy.

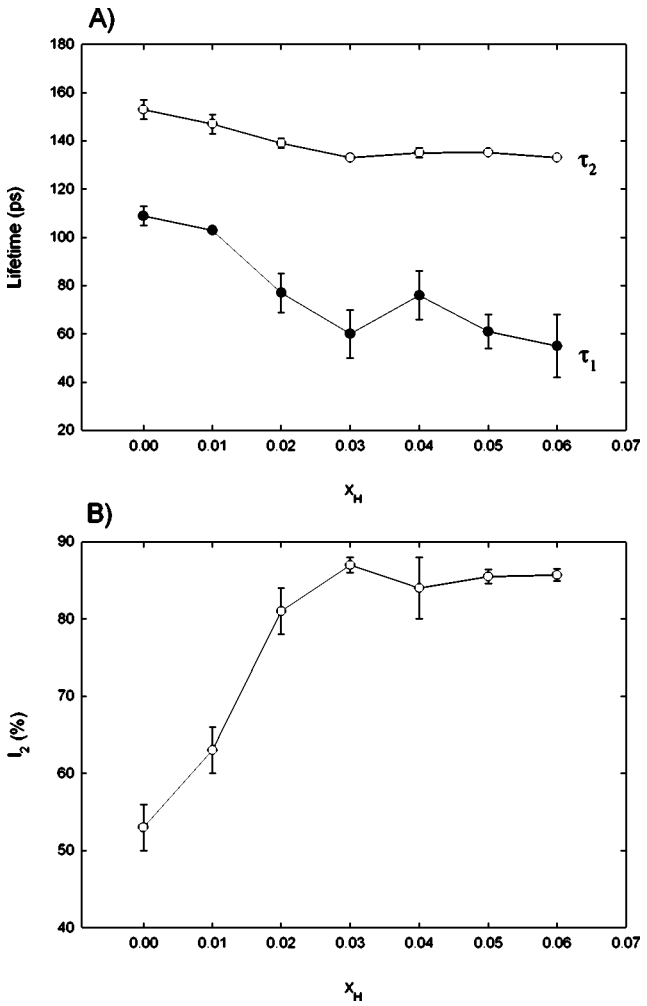


FIG. 4. (a) The lifetimes $\tau_1$ and $\tau_2$ of the exponential components resolved in the PL spectra for the Nb sample annealed at 850°C as a function of the hydrogen concentration $x_H$. (b) Dependence of the relative intensity $I_2$ on the hydrogen concentration for the Nb sample annealed at 850°C.

It reflects the fact that a fraction of positrons, which diffuses back to the surface and annihilates there, decreases with $E$, i.e., with increasing positron penetration depth. The $S(E)$ curve converges to a plateau at higher energies. It corresponds to a situation when all positrons annihilate in the bulk Nb and the contribution of positrons diffusing back to the surface is negligible. The $S(E)$ dependence can be well fitted by the VEPFIT program (model 5);[18] see the corresponding solid lines in Fig. 5. The fit resulted in a positron diffusion length $L_+ = 319 \pm 8$ nm.

The $S(E)$ curves for the Nb sample annealed at 1000°C loaded with hydrogen are shown in Fig. 5 as well. Contrary to the virgin sample, the hydrogen loaded samples were covered by the thin Pd overlayer. The local minimum of $S$ around 2 keV is due to positron annihilations in the thin Pd overlayer as was confirmed by a comparison with a reference 1.5 $\mu$m thick Pd film. One can clearly see that $S$ for bulk Nb, i.e., the plateau of the $S(E)$ dependence at high energies, remarkably increases with hydrogen concentration $x_H$. All the measured $S(E)$ curves were fitted by the VEPFIT program using a two-layer model, i.e., layer 1 for the thin Pd overlayer and layer 2 for bulk Nb. The fitted curves are plotted by solid lines in Fig. 5. $S$ and the positron diffusion length $L_+$ obtained for bulk Nb from the fits of the SPIS data are shown in Fig. 6. It is reasonable that $S$ for the bulk Nb increases with increasing hydrogen concentration. For the sample loaded above $x_H = 0.04$ no further increase of $S$ for bulk Nb can be seen. Contrary, $L_+$ decreases with increasing hydrogen concentration. Both the increase of $S$ and the decrease of $L_+$ give a clear indication for an increasing number of defects in the sample. Thus, the SPIS results agree quite well with the results of PL measurements and support the picture that new hydrogen-induced defects are created in hydrogenated samples and their concentration increases with increasing amount of hydrogen within the $\alpha$-phase region. Moreover, the SPIS results give direct evidence that the introduction of hydrogen-induced defects is not only a surface effect, but the defects are created in bulk of the Nb samples.

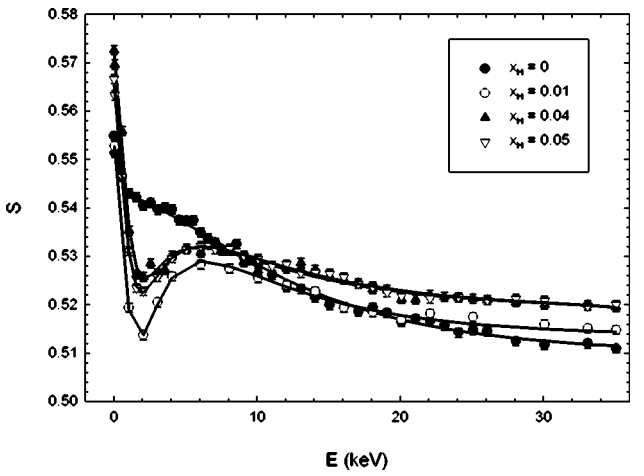


FIG. 5. $S(E)$ curves for the Nb sample annealed at 1000°C as a function of hydrogen concentration $x_H$. The solid lines show fits of the corresponding $S(E)$ dependencies by VEPFIT.

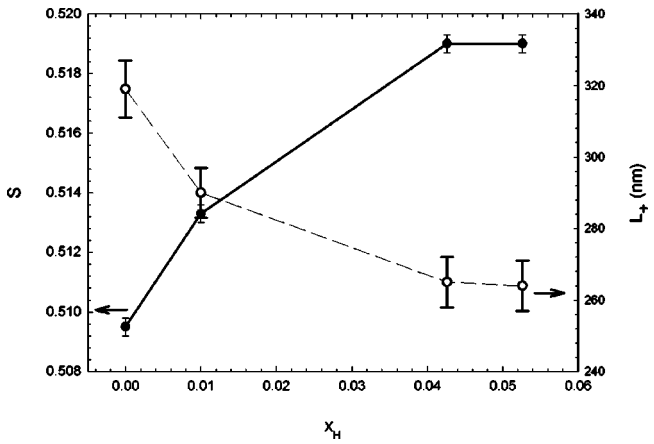


FIG. 6. $S$ parameter (full circles) and positron diffusion length $L_+$ (open circles) for bulk Nb as a function of hydrogen concentration $x_H$. $S$ and $L_+$ were obtained from fits of the $S(E)$ curves measured on the Nb sample annealed at 1000°C.

## IV. THEORY

Theoretical calculations were performed using the atom superposition method (ATSUP) in the same way as described in Ref. 27. The positron potential was constructed from the full lattice electrostatic potential and a local-density approximation (LDA) for the electron–positron correlation potential.[28] The crystalline charge density and Coulomb potential were approximated by superimposing the free atomic densities.[27] The Schrödinger equation for positrons was solved on three-dimensional grid points by the conjugate gradient method.[29] In this way the energy eigenvalue and the positron wave function $\psi_+(\mathbf{r})$ were obtained. The positron annihilation rate was calculated from

$$\lambda = \pi r_0^2 c \int n_+(\mathbf{r}) n_-(\mathbf{r}) \gamma(n_-(\mathbf{r})) d\mathbf{r}, \tag{4}$$

where $r_0$ is the classical electron radius and $c$ is the speed of light. The symbols $n_-(\mathbf{r})$ and $n_+(\mathbf{r}) = |\psi_+(\mathbf{r})|^2$ denote the electron and positron density, respectively. The enhancement factor $\gamma$ reflects an enhancement of the electron density at the site of the positron, which is due to the attractive electron–positron correlation. In the present calculations we used the parametrization of $\gamma$ introduced by Boroński and Nieminen.[29]

The calculations were performed for a supercell containing 256 Nb atoms using periodical boundary conditions for the positron wave function. One Nb atom was removed from the supercell for the calculation of lifetime of positrons trapped in a monovacancy. In addition, a corresponding number of hydrogen atoms was added for the calculations of positron lifetimes for vacancy–hydrogen complexes. Recent investigations regarding the convergence of calculated positron parameters with respect to the supercell sizes have shown that the supercell size used in the present calculations can be considered as sufficiently large for such point defect calculations.[30] The estimated uncertainty of the calculated lifetimes is about 10%.

A positron bulk lifetime $\tau_B = 126$ ps was obtained from the calculations. It agrees well with the experimental lifetime measured on the Nb sample annealed at 1000 °C; see Sec. III A. The calculated lifetime $\tau_B$ exhibits also good agreement with the lifetime of 125 ps calculated using a finite-element approach for the solution of the Schrödinger equation.[20]

A lifetime of positrons trapped in a Nb-monovacancy $\tau_v = 222$ ps was calculated. Clearly, $\tau_v$ is remarkably longer than the lifetime $\tau_2$ measured on the virgin sample of Nb annealed at 850 °C; see Sec. III A. It supports the picture discussed that positrons are trapped at dislocations in this virgin sample.

The experimental lifetime of positrons trapped at hydrogen-induced defects, see Figs. 3, 4, is significantly shorter than the calculated lifetime $\tau_v$ of positrons trapped at a Nb monovacancy. It means that the free volume of the hydrogen-induced defect is smaller than the monovacancy free volume. We consider that it is due to the hydrogen atom or atoms bound to a vacancy; see Sec. III B. In order to model positron trapping in a vacancy associated with one or more hydrogen atoms, we performed theoretical calculations for such vacancy–hydrogen complexes too.

As a first step, the position of the hydrogen atom associated with a vacancy in Nb has to be determined. It is well known that there is positive binding energy of hydrogen to a vacancy.[3,4] The position of a hydrogen atom bound to a vacancy can be calculated using the effective medium theory described in detail in Refs. 4 and 31. The basic idea of this theory is to replace the low-symmetry host by an effective high-symmetry host consisting of a homogeneous electron gas of a density equal to that seen by the embedded atom. The binding energy $\Delta E$ of an atom (hydrogen) to a host (Nb) is given [4] by

$$\Delta E(\boldsymbol{r}) = \Delta E_{\mathrm{eff}}^{\mathrm{hom}}(\overline{n_0}(\boldsymbol{r})) + \Delta E^{\mathrm{hyb}}(\boldsymbol{r}). \tag{5}$$

$\Delta E_{\mathrm{eff}}^{\mathrm{hom}}$ is the hydrogen binding energy in a homogeneous electron gas of a density seen by the hydrogen atom. This first term is dominating. $\Delta E_{\mathrm{eff}}^{\mathrm{hom}}$ characterizes the embedded atom. The properties of the host material are included in the calculation by spatial distributon of the electrom density $\overline{n_0}(\boldsymbol{r})$. Thus, the function $\Delta E_{\mathrm{eff}}^{\mathrm{hom}}$ can be calculated once and for all for a certain atom of interest independently on the host material. A parametrized form of $\Delta E_{\mathrm{eff}}^{\mathrm{hom}}$ for hydrogen was published in Ref. 32. The second term $\Delta E^{\mathrm{hyb}}$ in Eq. (5) is a correction term for hybridization. It was calculated in the frame of perturbation theory.[4] In the present work we used only the first term in the calculations. The electron density $n_0(\boldsymbol{r})$ of the host metal was approximated by a sum of atomic densities. The electron gas density $\overline{n_0}(\boldsymbol{r})$ is chosen as an average of the host electron density $n_0(\boldsymbol{r})$ over the electrostatic potential of the hydrogen atom placed at position $\boldsymbol{r}$ (see Refs. 4 and 31). A cutting radius $R_{\mathrm{cut}} = 1.3$ Å was used in the calculation of $\overline{n_0}$ (see Ref. 4).

As a test of the calculation procedure the binding energy $\Delta E_{\mathrm{eff}}^{\mathrm{hom}}$ of hydrogen in Nb was calculated first for a perfect defect-free Nb host lattice. A contour plot of $\Delta E_{\mathrm{eff}}^{\mathrm{hom}}$ in the (001) plane of the Nb lattice is shown in Fig. 7. As one can see in Fig. 7, $\Delta E_{\mathrm{eff}}^{\mathrm{hom}}$ exhibits minima in the (001) plane at tetrahedral interstitial positions, i.e., $\pm\frac{1}{4}, \pm\frac{1}{2}, 0$ and $\pm\frac{1}{2}, \pm\frac{1}{4}, 0$, for perfect Nb. Thus, the calculations give satisfactorily results for defect-free Nb.

The binding energy $\Delta E_{\mathrm{eff}}^{\mathrm{hom}}$ for hydrogen embedded in Nb with a vacancy in the 1,1,0 position was calculated. The results in the (001) plane are plotted in Fig. 8. One can see (Fig. 8) that the hydrogen atom is indeed bound to the vacancy. Positions with low values of $\Delta E_{\mathrm{eff}}^{\mathrm{hom}}$ are situated in a ring around the vacancy. The hydrogen atom is bound to the vacancy, however, it is not situated directly inside the vacancy like, e.g., a positron trapped in a vacancy. The hydrogen atom is anchored at a distance of about 1 Å from the vacancy. Six crystallographically equivalent positions with lowest energy $\Delta E_{\mathrm{eff}}^{\mathrm{hom}}$ were obtained from the calculations: 0.64(2),1.00(2),0.00(2); 1.36(2),1.00(2),0.00(2); 1.00(2),0.64(2),0.00(2); 1.00(2),1.36(2),0.00(2); 1.00(2), 1.00(2),±0.64(2) (uncertainties of the determination of the positions are given in parentheses). We note that the coordinates are given in fractions of basic lattice translations and

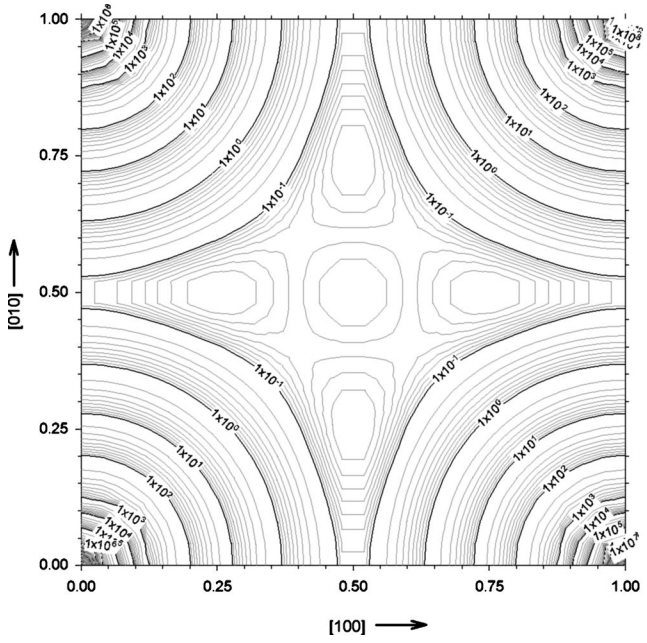


FIG. 7. The binding energy $\Delta E_{\mathrm{eff}}^{\mathrm{hom}}$ in the (001) plane for hydrogen in perfect, defect-free Nb, calculated using the effective medium theory. For details of calculations see the text. Note that a constant factor of 2.0 eV was added to all calculated binding energies in order to shift them to positive numbers to scale the contours in the logarithmic scale, i.e., the contours are equally separated in the logarithmic scale. It was done only to present graphically the calculted results in a convenient form. The coordinates in the $x$ and $y$ axis are given in fractions of the Nb lattice parameter $a = 3.3033$ Å.

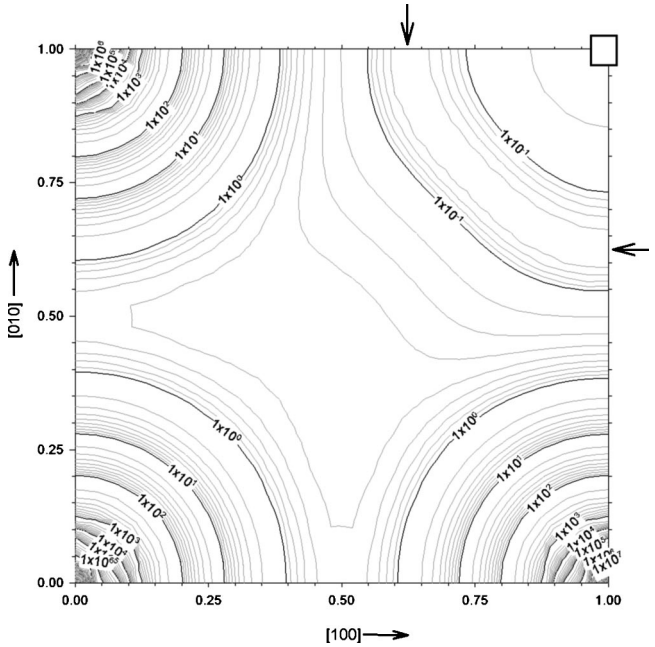


FIG. 8. The binding energy $\Delta E_{\mathrm{eff}}^{\mathrm{hom}}$ in the (001) plane for hydrogen in Nb with vacancy in the 1,1,0 position (indicated schematically by an open square). $\Delta E_{\mathrm{eff}}^{\mathrm{hom}}$ was calculated using the effective medium theory. For details of the calculations see the text. A constant factor of 2.5 eV was added to all calculated binding energies in order to shift them to positive values and to plot the contours in logarithmic scale. It was done only to present graphically the calculted results in a convenient form. The positions with low energy $\Delta E_{\mathrm{eff}}^{\mathrm{hom}}$ are situated in a ring surrounding the vacancy. The position of the ring is indicated by arrows. The coordinates in the $x$ and $y$ axis are given in fractions of the Nb lattice parameter $a = 3.3033$ Å.

the vacancy is placed in a 1,1,0 position. The calculated equilibrium positions of a hydrogen atom bound to a vacancy in Nb can be described so that the hydrogen atom is displaced $0.46 \pm 0.07$ Å from the nearest-neighbor octahedral position towards the vacancy site. A schematic diagram of one of the calculated hydrogen positions is shown in Fig. 9. Myers, Picraux and Stolz[33] found that deuterium bound to a vacancy in Fe is displaced 0.4 Å from the nearest-neighbor octahedral site. Effective medium calculations for Fe resulted in virtually the same result with displacement $0.5 \pm 0.1$ Å from the octahedral position.[32] Both Nb and Fe exhibit bcc structure, therefore relatively similar results obtained for both metals seem to be quite reasonable.

The positron density in the (001) plane for Nb with a vacancy in the 1,1,0 position associated with a hydrogen at the 0.64,1,0 position, i.e., one of the six crystallographically equivalent positions calculated by the effective medium theory, is shown in Fig. 10. One can see that the positron is localized at the site of the vacancy. Thus obviously, the vacancy associated with a hydrogen atom is capable of positron trapping. An opposite situation occurs for vacancy–carbon pairs in Fe,[34,35] which are not able to trap positrons. The lifetime of a positron trapped at a Nb vacancy associated with a single hydrogen atom was calculated to be $\tau_{\mathrm{H-v}} = 204$ ps. Hence, $\tau_{\mathrm{H-v}}$ is remarkably shorter than the lifetime $\tau_v$ of positrons trapped at a vacancy without hydrogen. It is a consequence of smaller free volume and enhanced electron density due to the added hydrogen atom.

On the other hand, the calculated lifetime $\tau_{\mathrm{H-v}}$, is significantly higher than the lifetime of positrons trapped at hydrogen-induced defects observed in experiments for all the studied Nb samples. Thus, the free volume of the hydrogen-induced defect has to be significantly lower than the free

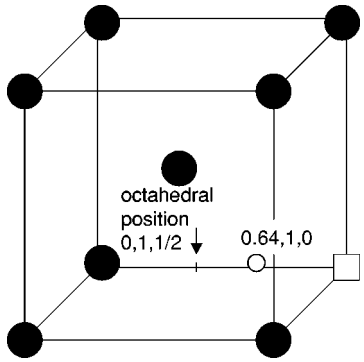


FIG. 9. A schematic diagram of position of hydrogen atom bound to a vacancy calculated using the efective medium theory. The hydrogen atom is denoted by an open circle, while Nb atoms are plotted by filled circles. The vacancy depicted by an open square is placed at the 1,1,0 position. The hydrogen atom bound to the vacancy is displaced 0.46 Å from the nearest neighbor octahedral interstitial position (denoted by an arrow) towards the vacancy.

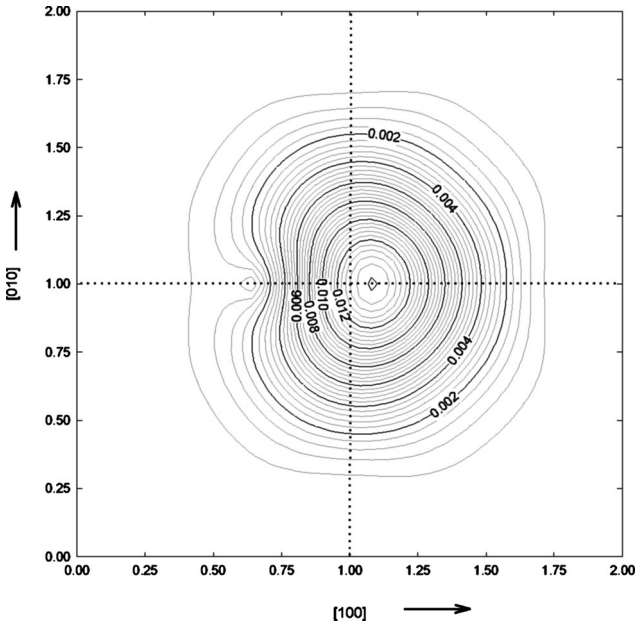


FIG. 10. The calculated positron density in (001) plane for Nb with a vacancy associated with a single hydrogen atom. Four unit cells are shown in the figure. The cell boundaries are shown by the dotted lines. The vacancy is situated at the 1,1,0 position. The hydrogen atom is placed at the 0.64,1,0 position calculated using the effective medium theory. The coordinates are given in fractions of the Nb lattice parameter $a=3.3033$ Å.

volume of a vacancy associated with single hydrogen atom. It indicates that vacancies associated with more than one hydrogen atom were likely created in the studied Nb samples by hydrogen loading. In order to obtain information about how hydrogen atoms surrounding a vacancy influence the lifetime of trapped positrons, we performed further calculations of positron lifetime as a function of number of hydrogen atoms associated with the vacancy. We gradually filled the six crystallographically equivalent positions with minimum $\Delta E_{\mathrm{eff}}^{\mathrm{hom}}$ obtained using the effective medium theory (see above) with hydrogen atoms and the lifetimes of positrons trapped at such vacancy–hydrogen complexes were calculated. It should be pointed out that this is only a rough approximation because the hydrogen–hydrogen interaction is neglected. Nevertheless, the hydrogen interaction with the vacancy is dominant and even such a simple approximation can give us an estimation of the dependence of the lifetime of trapped positrons on the number of hydrogen atoms bound to the vacancy. Results are plotted in Fig. 11. As one can see, the positron lifetime remarkably decreases with the number of hydrogen atoms surrounding the vacancy. In the case, when all the six crystallographically equivalent positions are filled by hydrogen, the lifetime even approaches the Nb bulk positron lifetime. The calculated binding energy of the positron to the vacancy is plotted as a function of number of hydrogen atoms surrounding the vacancy in Fig. 11 as well. The positron binding energy strongly decreases with the number of hydrogen atoms surrounding the vacancy. One can see that the binding energy of the positron to a vacancy surrounded by six hydrogen atoms falls below 0.2 eV, i.e., the detrapping of positrons trapped at such vacancy–

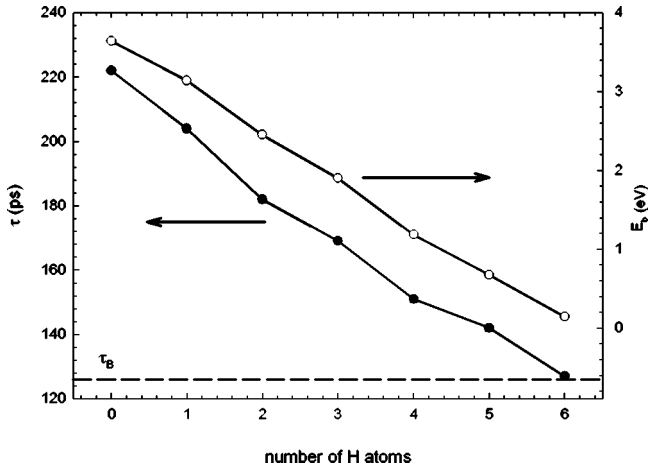


FIG. 11. Calculated lifetime $\tau$ and binding energy $E_b$ of positrons trapped in a Nb vacancy as a function of the number of hydrogen atoms surrounding the vacancy. The Nb bulk lifetime is plotted by the dashed line.

hydrogen complexes might play an important role already at room temperature.

A lifetime $\tau_2 \approx 150$ ps of positrons trapped at hydrogen-induced defects was observed on the Nb samples annealed at 1000 °C, see Sec. III B. If we compare this experimental lifetime with the theoretical calculations, it is clear that it corresponds well with the case of a vacancy surrounded by four hydrogen atoms; see Fig. 11. Thus, we can conclude that vacancies associated with four hydrogen atoms were likely created due to hydrogen loading in the Nb sample annealed at 1000 °C. One can consider that once a hydrogen–vacancy pair is created, it is quickly surrounded also by additional hydrogen atoms, because of their high mobility. A complex consisting of a vacancy surrounded with more than four hydrogen atoms becomes likely unstable due to the repulsive interaction of the hydrogen atoms. As a consequence, vacancies associated with four hydrogen atoms represent the most probable configuration of hydrogen-induced defects. The situation is the most unambiguous in case of the Nb sample annealed at 1000 °C, because it can be considered as defect-free in the virgin state prior to hydrogen loading. The picture given above is consistent with atom embedding calculations for hydrogen binding to vacancies in nickel.[36] These calculations yield about 5 hydrogen atoms bound to one vacancy.

A more complex situation occurs in the Nb sample annealed at 850 °C, which contains dislocations already in the virgin state. As one can see in Fig. 4, $\tau_2$ slightly decreases during hydrogen loading from 150 ps down to 140 ps. The component with lifetime $\tau_2$ represents a mixture of positrons trapped at dislocations present already in the virgin sample and positrons trapped in the hydrogen-induced defects. The decrease of $\tau_2$ could be an indication that hydrogen is bound also to vacancies anchored in the vicinity of a dislocation line. This should lead to a decrease of the lifetime of positrons trapped at dislocations, see Sec. I, and therefore, also to a decrease of $\tau_2$.

The binding energy of a hydrogen atom to a Nb vacancy $E_b^{\mathrm{H-v}}=0.50$ eV can be obtained from the effective medium theory calculations as the difference between the energy of

hydrogen in the tetrahedral interstitial site and the hydrogen bound to a vacancy. The vacancy formation energy $E_f = 2.32$ eV was calculated for Nb using first-principles calculations.[37] The energy $E_f$ is significantly reduced due to the presence of diluted interstitial hydrogen. For example, the formation energy is decreased down to $E_f - E_b^{\mathrm{H-v}} = 1.82$ eV for a vacancy–hydrogen pair. An order-of-magnitude estimation (neglecting the hydrogen–hydrogen interaction) of the formation energy for a vacancy surrounded by 4 hydrogen atoms yields $E_f - 4E_b^{\mathrm{H-v}} = 0.32$ eV.

The equilibrium concentration of vacancies associated with 4 hydrogen atoms can be estimated using the relation

$$c \approx p e^{S_f/k} e^{-(E_f - 4E_b^{\mathrm{H-v}})/kT}, \tag{6}$$

with $S_f = (2-3)k$ known to hold for the formation entropy of a vacancy in many metals.[38] In the present work we used $S_f \approx 2.3k$, which gives $e^{S_f/k} \approx 10$. The quantity $p$ denotes the probability that 4 H atoms are situated in the vicinity of the vacancy. In the case of substitutional impurities, it is necessary to have 4 impurity atoms situated at the nearest neighbor positions around a certain atom to form a complex consisting of the vacancy and the 4 impurity atoms. The reason is that the substitutional impurities usually exhibit a low mobility, i.e., they can change position only by vacancy-assisted diffusion. If we apply the same condition to hydrogen, i.e., if we assume that to form a V–4H complex (a vacancy surrounded by 4 hydrogen atoms), it is required to have 4 H atoms situated at the nearest neighbor interstitial positions around a Nb atom, then $p \sim (c_{\mathrm{H}})^4$, where $c_{\mathrm{H}}$ represents the atomic concentration of hydrogen. Under this condition an equilibrium concentration of V–4H complexes at room temperature $c \approx 7 \times 10^{-9}$ at.% is obtained from Eq. (6). This concentration is extremely low being four orders of magnitude below the lower sensitivity limit of positron annihilation spectroscopy.[21]

However, contrary to the substitutional impurities, interstitial hydrogen is highly mobile. As a consequence it is not necessary to have hydrogen atoms situated at the nearest neighbor interstitial positions. In our opinion a more realistic picture is to assume that to form a V–4H complex it is necessary to have at least four hydrogen atoms situated in a certain "active volume" $V_0$ around a vacancy, when the vacancy is formed. We assume that there is a long-range interaction between the interstitial hydrogen atoms and the vacancy due to long-range elastic distortion of the lattice caused by hydrogen. $V_0$ has to be small enough to allow for the mutual interaction of H and vacancy and can be estimated from our PAS results.

One can see in Fig. 3(b) that the concentration of hydrogen-induced defects in the Nb sample annealed at 1000 °C saturates at a hydrogen concentration $x_{\mathrm{H}}$ in the interval 0.02–0.03 [H/Nb]. A similar behavior is observed in the Nb sample annealed at 850 °C; see Fig. 4(b). Hence, from $x_{\mathrm{H}} \approx 0.025$ the concentration of diluted interstitial H is high enough and the equilibrium concentration of V–4H complexes does not depend on hydrogen concentration anymore. Once a vacancy is created, there are always at least 4 H atoms in the vicinity of the vacancy, i.e., in $V_0$. From this assumption we can estimate $V_0$. At a hydrogen concentration $x_{\mathrm{H}} \approx 0.025$ we have *on average* 4 H atoms in $V_0$, i.e. $c_{\mathrm{H}} V_0 = 4$, where $c_{\mathrm{H}} = 1.4 \times 10^{21}$ cm$^{-3}$ is the volume concentration of hydrogen corresponding to $x_{\mathrm{H}} \approx 0.025$ [H/Nb]. Thus, we obtain $V_0 = 2.9$ nm$^3$, which corresponds to about 80 unit cells of Nb. Let us distinguish now two possibilities: (i) For $x_{\mathrm{H}} \geqslant 0.025$, we have on average at least 4 H atoms in the active volume $V_0$ around a vacancy. It means, that the probability $p$ in Eq. (6) equals 1. (ii) For $x_{\mathrm{H}} < 0.025$, there are *on average* less than 4 atoms in $V_0$. It can be shown that the probability $p$ is given by the expression

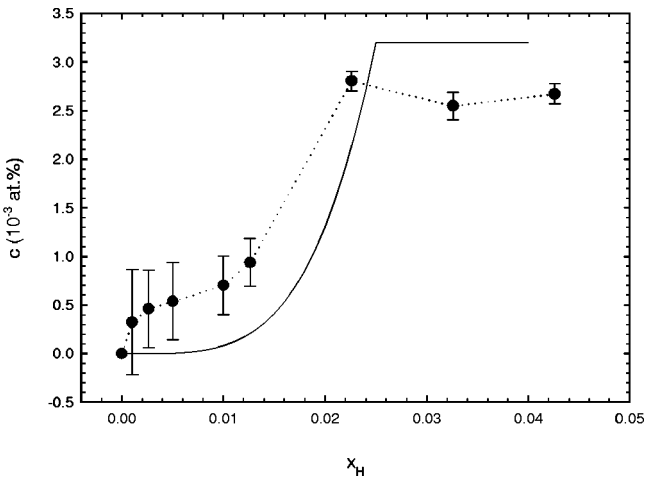


FIG. 12. The concentration of hydrogen-induced vacancy–hydrogen complexes in the Nb sample annealed at 1000 °C estimated from experimental data using Eq. (3) is shown by filled circles connected by a dotted line. The estimated equilibrium concentration of vacancy–4H complexes calculated using Eq. (6), with the probability $p$ given by Eq. (7) for $x_{\mathrm{H}} < 0.025$ and $p = 1$ for $x_{\mathrm{H}} \geqslant 0.025$ is plotted by a solid line.

$$p = \frac{\frac{1}{x_{\mathrm{H0}}}\left(\frac{4q}{x_{\mathrm{H0}}} - 1\right)\left(\frac{4q}{x_{\mathrm{H0}}} - 2\right)\left(\frac{4q}{x_{\mathrm{H0}}} - 3\right)}{\frac{1}{x_{\mathrm{H}}}\left(\frac{4q}{x_{\mathrm{H}}} - 1\right)\left(\frac{4q}{x_{\mathrm{H}}} - 2\right)\left(\frac{4q}{x_{\mathrm{H}}} - 3\right)}, \tag{7}$$

where $x_{\mathrm{H0}} = 0.025$ and $q = 6$ represent the number of tetrahedral interstitial sites per Nb atom. The concentration of V–4H complexes calculated using Eq. (6) with $p$ given by Eq. (7) for $x_{\mathrm{H}} < 0.025$ and $p = 1$ for $x_{\mathrm{H}} \geqslant 0.025$ is plotted in Fig. 12 by a solid line. It is compared with the measured concentration of the hydrogen induced defects in the Nb sample annealed at 1000 °C determined using Eq. (3). The specific trapping rate $\nu_{\mathrm{H-v}} = 1 \times 10^{14}$ s$^{-1}$ at. was used, i.e., the value at lower part of the interval of the specific trapping rates typical for a monovacancy in most metals. The reason is that we expect a lowering of the specific trapping rate due to the presence of bound H atoms.

Taking into account that both concentration dependencies plotted in Fig. 12 were obtained using rather rough estimations, we conclude that they exhibit satisfactory agreement. Moreover, the simple model described above explains at least qualitatively the observed dependence of the density of the hydrogen-induced defect on hydrogen concentration, i.e.,

an increase at low $x_H$ and then a saturation above a certain hydrogen concentration $x_{H0}$. On the other hand, it is not possible to explain the experimental results by formation of hydrogen-induced vacancies using the assumption that H atoms must be situated at the nearest neighbor interstitial positions to form a vacancy–hydrogen complex (see the discussion above).

Equation (6) with $p=1$ was used also by Birnbaum *et al.* in Ref. 39 to estimate the concentration of vacancy–hydrogen complexes in Al created by hydrogen charging at room temperature. The authors obtained a good agreement with the concentration determined experimentally by length change and lattice parameter measurements. The hydrogen concentration in the Al samples was $c_H \sim 10^{-3}$. Thus, assuming that there must be at least one H atom in $V_0$ around a vacancy, one obtains $V_0 \sim 250$ unit cells. It is comparable in order of magnitude to our result in Nb. On the other hand, the assumption that H must be situated at the nearest neighbor interstitial position to form a V–H complex gives a negligible concentration of vacancy–hydrogen complexes, which is contradictory to the experimental finding. It should be noted that Fukai *et al.* in Ref. 40 used Eq. (6) with $p=1$ to estimate the concentration of V–nH complexes created in Pd under high hydrogen pressures and high temperatures. Again this approach gives good agreement with experiment. However, in that case the hydrogen concentration in the sample was high, $c_H \sim 1$. We think that a successful use of Eq. (6) for an estimation of the equilibrium concentration of vacancy–hydrogen complexes in other H-metal systems gives an additional support for using it in the present work.

The formation of lattice vacancy at the surface accompanying the introduction of a H solute, followed by the diffusion of the H–vacancy complex into the volume, was reported for hydrogen-loaded Al at room temperature.[39] The hydrogen-induced vacancies in Nb samples studied in the present work could be created at the external surface as well as at internal surfaces like grain boundaries. One would expect that H influences the mobility of the created vacancies. However, from the present set of data we cannot judge if the vacancies are introduced at the surfaces or at internal vacancy sources.

## V. CONCLUSIONS

Investigations of defects in Nb bulk samples step-by-step loaded by hydrogen in the $\alpha$-phase concentration range were performed in the present work. We have found that hydrogen-induced defects are created in Nb during hydrogen loading. The concentration of hydrogen-induced defects increases with an increasing amount of hydrogen with a saturation above a certain hydrogen concentration. Comparisons with theoretical calculations have revealed that vacancies surrounded by four hydrogen atoms are most probably introduced due to the hydrogen loading. Simple estimations indicate that the formation of hydrogen-induced vacancies could be due to a significant decrease of the vacancy formation energy in the hydrogen-loaded Nb. Additional theoretical work is desirable in future in order to derive a more detailed model of hydrogen-induced defect formation.

## ACKNOWLEDGMENTS

Extended stays of Jakub Čížek at University Göttingen and Forschungszentrum Rossendorf were supported by The Alexander von Humboldt Foundation. Authors are grateful to their unknown referees for their encouraging and stimulating remarks to further improve the theoretical discussion of this work.

*Electronic mail: jcizek@mbox.troja.mff.cuni.cz

[1] J. Völkl and G. Alefeld, in *Hydrogen in Metals I*, Topics in Applied Physics, edited by G. Alefeld and J. Völkl (Springer-Verlag, Berlin, 1978), Vol. 28, p. 321.
[2] A. Cracknell, Chem. Eng. J. **306**, 92 (1976).
[3] B. Lengeler, S. Mantl, and W. Triftshäuser, J. Phys. F: Met. Phys. **8**, 1691 (1978).
[4] J. Nørskov, Phys. Rev. B **26**, 2875 (1982).
[5] R. Kirchheim, Prog. Mater. Sci. **32**, 261 (1988).
[6] W. Rudzińska, J. Pajak, C. Szymański, and R. Szatanik, Acta Phys. Pol. A **99**, 479 (2001).
[7] Y. Shirai, H. Araki, T. Mori, W. Nakamura, and K. Sakaki, J. Alloys Compd. **330**, 125 (2002).
[8] T. Schober and H. Wenzl, in *Hydrogen in Metals II*, Topics in Applied Physics, edited by G. Alefeld and J. Völkl (Springer-Verlag, Berlin, 1978), Vol. 29, p. 32.
[9] T. Schober, Phys. Status Solidi A **30**, 107 (1975).
[10] P. Hautojärvi, in *Positrons in Solids*, edited by P. Hautojärvi (Springer-Verlag, Berlin, 1979), p. 1.
[11] A. van Veen, H. Schut, and P. Mijnarends, in *Positron Beams and their Applications*, edited by P. Coleman (World Scientific, Singapore, 2000), p. 191.
[12] Y. Fukai, *The Metal–Hydrogen System*, Springer Series in Materials Science (Springer-Verlag, Berlin, 1993), Vol. 21.
[13] R. Kirchheim, F. Sommer, and G. Schluckebier, Acta Metall. **30**, 1059 (1982).
[14] F. Bečvář, J. Čížek, L. Lešták, I. Novotný, I. Procházka, and F. Šebesta, Nucl. Instrum. Methods Phys. Res. A **443**, 557 (2000).
[15] F. Bečvář, J. Čížek, and I. Procházka, Acta Phys. Pol. A **95**, 448 (1999).
[16] I. Procházka, I. Novotný, and F. Bečvář, Mater. Sci. Forum **255-257**, 772 (1997).
[17] W. Anwand, H.-R. Kissener, and G. Brauer, Acta Phys. Pol. A **88**, 7 (1995).
[18] A. van Veen, H. Schut, M. Clement, J. de Nijs, A. Kruseman, and M. IJpma, Appl. Surf. Sci. **85**, 216 (1995).
[19] ICDD (International Centre for Diffraction Data), Powder Diffraction Pattern Database, PDF-2.
[20] P. Sterne, J. Pask, and B. Klein, Appl. Surf. Sci. **149**, 238 (1999).
[21] P. Hautojärvi and C. Corbel, in *Proceedings of the International School of Physics 'Enrico Fermi', Course CXXV*, edited by A. Dupasqier and A. Mills (IOS Press, Varenna, 1995), p. 491.
[22] L. Smedskjaer, M. Manninen, and M. Fluss, J. Phys. F: Met. Phys. **10**, 2237 (1980).

[23] H. Peisl, in *Hydrogen in Metals I*, *Topics in Applied Physics*, edited by G. Alefeld and J. Völkl (Springer-Verlag, Berlin, 1978), Vol. 28, p. 53.
[24] R. Kirchheim, Acta Metall. **30**, 1069 (1982).
[25] J. de Vries, Ph.D. thesis, Technical University Delft, 1987.
[26] R. West, in *Positrons in Solids*, edited by P. Hautojärvi (Springer-Verlag, Berlin, 1979), p. 89.
[27] M. Puska and R. Nieminen, J. Phys. F: Met. Phys. **13**, 333 (1983).
[28] J. Arponen and E. Pajane, Ann. Phys. (N.Y.) **121**, 343 (1979).
[29] E. Boroński and R. Nieminen, Phys. Rev. B **34**, 3820 (1986).
[30] T. Korhonen, M. Puska, and R. Nieminen, Phys. Rev. B **54**, 15 016 (1996).
[31] M. Stott and E. Zaremba, Phys. Rev. B **22**, 1564 (1980).
[32] J. Nørskov, F. Besenbacher, J. Bøttiger, B. Nielsen, and A. Pisarev, Phys. Rev. Lett. **49**, 1420 (1982).
[33] S. M. Myers, S. Picraux, and R. Stolz, J. Appl. Phys. **50**, 5710 (1981).
[34] A. Vehanen, P. Hautojärvi, J. Johansson, and J. Yli-Kauppila, Phys. Rev. B **25**, 762 (1982).
[35] P. Hautojärvi, L. Pöllänen, A. Vehanen, and J. Yli-Kauppila, J. Nucl. Mater. **114**, 250 (1983).
[36] S. Myers, Phys. Rev. B **33**, 854 (1986).
[37] P. Korzhavyi, I. Abrikosov, B. Johansson, A. Ruban, and H. Skriver, Phys. Rev. B **59**, 11 693 (1999).
[38] H. Wollenberger, in *Physical Metalurgy*, edited by R. Cahn and P. Hansen (North-Holland, Amsterdam, 1983), Vol. 2, p. 1146.
[39] H. Birnbaum, C. Buckley, F. Zeides, E. Sirois, P. Rozenak, S. Spooner, and J. Lin, J. Alloys Compd. **253-254**, 260 (1997).
[40] Y. Fukai and N. Okuma, Phys. Rev. Lett. **73**, 1640 (1994).